JOURNAL OF CATALYSIS **178,** 84–93 (1998)
ARTICLE NO. CA982129

Characterization of Supported Ruthenium Catalysts Derived from Reaction of $Ru_3(CO)_{12}$ with Rare Earth Oxides

Linda A. Bruce, Manh Hoang,[1] Anthony E. Hughes, and Terence W. Turney

C.S.I.R.O Manufacturing Science and Technology, Private Bag 33, Clayton South MDC, Victoria, 3169, Australia

Received September 4, 1997; revised April 13, 1998; accepted April 28, 1998

The surface chemistry of supported ruthenium on high surface area (>50 m^2 g^{-1}) rare earth oxides (La, Ce, Pr, Tb, Ho, and Yb) has been studied by temperature-programmed reduction, temperature-programmed oxidation, X-ray photoelectron spectroscopy, Fourier transform infrared spectroscopy, and hydrogen chemisorption. Reduction of carbonyl ligands and surface carbonate by H_2 takes place in the range 255°C < T < 300°C, with evolution of CH_4 and formation of nanometer-sized Ru particles. The Ru nanocrystallites were readily oxidized to RuO_2, which strongly interacted with the support. Prolonged heating (6 h) in 1% O_2/He at 350°C led to loss of free RuO_2 from the support, but shorter term heating resulted in rearrangement of RuO_2 on the support, as revealed by alteration in the reduction profile with varying oxidation conditions. Hydrogen adsorption–desorption experiments showed that dispersion of Ru metal was increased by the reduction–oxidation–reduction cycle for La and Yb but not the other oxides. Facile reduction of Ce, Pr, and Tb oxides was attributed to the dissociative chemisorption of H_2 on Ru metal nanocrystallites, and spillover of atomic species to the support. Reducible oxides such as CeO_2 and Pr_6O_{11} have been found to be effective support for the production of lower alkene from synthesis gas.

Key Words: **characterisation of supported ruthenium catalyst; supported ruthenium on rare earth oxides; Fischer–Tropsch synthesis.**

INTRODUCTION

Numerous studies have been devoted to the influence of the support on the Ru catalyzed hydrogenation of CO (1–8). Support effects on catalyst performance can arise from alteration of the electronic characteristics of the active metal, or through promotion or inhibition of secondary reactions on the support itself. Thus, a characteristic of acidic supports is a rich carbonium ion chemistry, leading to numerous secondary reactions (e.g., chain branching, cracking, and hydrogenation reactions). In contrast, such reactions on basic supports are minimal.

A number of earlier studies have concentrated on MgO as a basic support for Ru-catalyzed CO hydrogenation, with very variable outcome as to the products (5–7). However, there are also studies on La_2O_3 and CeO_2, in which substantial lower olefin production has been reported (4, 7), demonstrating the expected relative inhibition of secondary carbonium ion rearrangements on a basic support. In particular, we have previously reported a high activity and stable Ru promoted Co/CeO_2 catalyst with good olefin selectivity and low CO_2 production (8). To better understand the performance of that $Ru/Co/CeO_2$ catalyst, we have undertaken a systematic study of the components and their interactions. Previous publications have reported our work on the synthesis of high area ceria and its surface and bulk properties as a function of area (9) and the interaction of $Ru_3(CO)_{12}$ with rare earth oxides to form surface Ru carbonyl species (10). This publication describes the reduction of those surface carbonyl species, their properties, and Fischer–Tropsch activity with subsequent publications examining the influence of CO_2 and H_2O on the catalyst.

A method for the preparation of rare earth oxides with high surface areas, between 50 and 200 m^2 g^{-1}, has been reported (11). These high surface area oxides introduce the possibility of designing catalysts which are likely to effect highly selective hydrogenation of carbon monoxide to unbranched lower olefins with minimal carbon dioxide formation. Thus, facile carbonation of the support by CO_2, produced in the water–gas shift reaction, to form rare earth carbonate species, becomes a likely reaction. For the rare earths of variable oxidation state, Ce, Pr, and Tb, reduction of the high area surface or of the bulk support itself can occur by H_2 spillover. In a previous paper Fourier transform infrared (FTIR) spectroscopy and X-ray photoelectron spectroscopy (XPS) were used to identify the surface species $[(OC)_2Ru(OM)_2]_n$ at 2 wt% Ru loading, and possibly $[Ru_3(\mu\text{-H})(CO)_{10}(\mu\text{-OM})]$ at 5% metal loadings (10). The present paper investigates the reduction of these surface species on La_2O_3, Ho_2O_3, Yb_2O_3, CeO_2, Pr_4O_7, Tb_4O_7, and their subsequent oxidation–reduction.

EXPERIMENTAL

Syntheses and characterization of high area M_2O_3 (M = La, Ho, and Yb), CeO_2, Pr_6O_{11}, and Tb_4O_7 powders are

[1] To whom correspondence should be addressed.

0021-9517/98 $25.00

reported elsewhere (9, 11). Ruthenium dodecacarbonyl was prepared from $RuCl_3$ and recrystallized from toluene (12). Solutions of $Ru_3(CO)_{12}$ in *n*-heptane (ca. 1 g/L) were reacted with the rare earth oxide (freshly calcined at 600°C) by stirring under N_2 at 21°C. After 24 h, the solid was filtered and washed with pure *n*-heptane before drying for ca. 1 h *in vacuo* (ca. 0.01 kPa) at 21°C to provide the catalyst precursor, which was stored under N_2.

X-ray photoelectron spectra (XPS) were measured with a Vacuum Generators ESCALAB using the Al anode operated at 150 W (pass energy 30 eV, 4 mm slits). Specimens were mounted onto Ni-plated Cu sample holders as loose powders. Treatments were done *in situ* in a flowthrough reaction cell (15 cm^3/min), using either 3% H_2/N_2 for reduction at 350°C or 1% O_2/He for oxidation at 150°C.

The Ru 3*d* doublet, C 1*s* hydrocarbon (CH_x), and carbonate (13) intensities were extracted from the C 1*s*–Ru 3*d* spectral envelope by a curve-fitting procedure based on damped nonlinear least squares optimization (14). For Ru/CeO_2 inclusion of an additional peak (C_{III} at ~291 eV) was required to fit the high binding energy region of C 1*s* satisfactorily. This peak had variable binding energy and was attributed to weakly adsorbed oxygenated carbon species (15). The Ru $3d_{5/2}$–$3d_{3/2}$ splitting was set to 4.1 eV (17). Splitting of 4.2 eV, also reported in the literature (18) was tested but found to make less than 0.05 eV difference in the binding energies and less than 10% difference in the intensities. The relative heights were varied according to whether the Ru was in a metallic state or oxidized. In the metallic state there is Coster–Kronig broadening of the Ru $3d_{3/2}$ peak compared to the Ru $3d_{5/2}$ peak (19); therefore a peak height ratio for Ru $3d_{3/2}$: Ru $3d_{5/2}$ of 0.588 was used to give the required area ratio (0.69) when the broader $3d_{3/2}$ peak was used in fitting. The peak FWHM of the Ru $3d_{3/2}$ was fixed at 0.43 wider than the Ru $3d_{5/2}$. For the oxidized state, the Coster–Kronig path which gives rise to the broadening is closed, and therefore the peak widths are identical for the spin–orbit pairy (19).

The spectrometer was calibrated using the Au $4f_{7/2}$ peak at 84.0 eV and the Cu $2p_{3/2}$ peak at 932.6 eV. Internal charge referencing for the Ru promoted lanthana and ceria systems is difficult because the C 1*s* is obscured by the Ru 3*d* doublet, and the rare earth oxide core lines have complex structures. Previously we have used the C 1*s* line (285.0 eV) after fitting the Ru 3*d*–C 1*s* region (10). In this study the carbonate peak positions were chosen as reference points since interference from the Ru 3*d* was minimal. Carbonate peak positions were measured in the absence of Ru on both lanthana and ceria as well as on cerium carbonate and oxycarbonate (Table 1). These positions were referred to the adventitious carbon at 285.0 eV. For the heavily carbonated materials (La_2O_3 and $Ce_2(CO_3)_3$), the binding energy was higher than for Ce_2OCO_3, which only had a small carbonate peak due to its volatility in vacuum (9). Thus for La_2O_3 and CeO_2, the carbonate peaks at 289.5 and 289.0 eV were chosen as the reference peaks, respectively. In the case of lanthana, the use of the carbonate as a reference gave a La $3d_{5/2}$ position of 834.5 ± 0.2 eV, which is in good agreement with reported values (20, 21).

TABLE 1

C 1*s* Binding Energies for Selected Compounds

Compound	C 1*s*
Carbonate-contaminated La_2O_3	289.5
$Ce_2(CO_3)_3$	289.2
$CeO(CO_3)$	288.6

For La_2O_3, the best fits to the O 1*s* region were obtained by using four components which were assigned to oxide oxygen, such as found in $La_2\underline{O}_3$ (~528.3 eV), La<u>O</u>OH (~529.5 eV), and carbonate oxygen (~530.8 eV), and to hydroxyl oxygen in La($\underline{O}H)_3$ (~531.8 eV) (22). For the CeO_2 catalysts the O 1*s* region was satisfactorily fitted using two components, oxide (O_I) and a combination of hydroxyl and carbonate oxygens (O_{II}). The spectroscopy of the Ce 3*d* region was complex due to a satellite structure for which precise assignment remains tentative (23). Generally, on fully oxidized ceria (Fig. 1a), the features labeled v, v″, and v‴ are accepted as corresponding to $3d^9 4f^2$, $3d^9 4f^1$, and

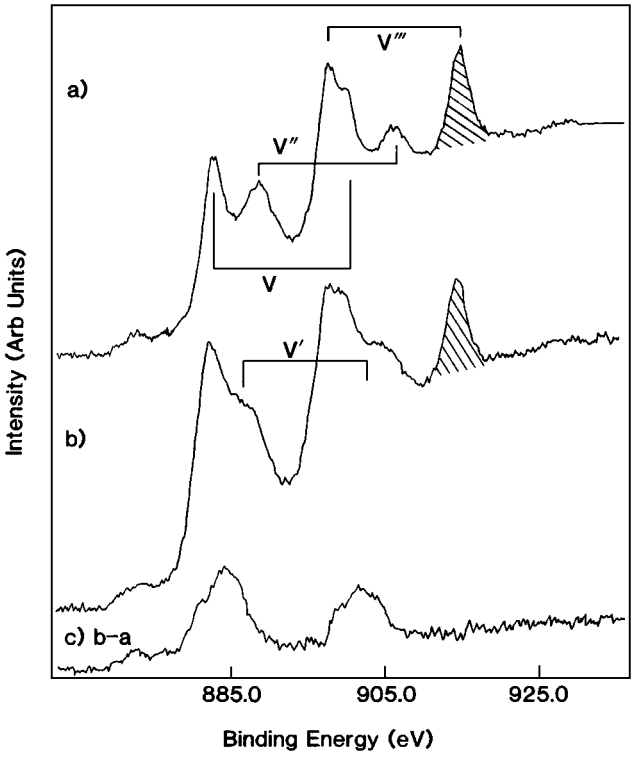

FIG. 1. XPS spectra for Ce 3*d* region of (a) fully oxidized 1.8 wt% Ru/CeO_2, (b) same sample after reduction at 350°C in 3% H_2/N_2 for 20 min, and (c) difference spectrum, (b) – (a), derived as described in the text.

$3d^9 4f^0$ final states, respectively ($3d_{5/2}$ and $3d_{3/2}$ splittings are designated by the joined lines) (24). For a partially reduced sample, a new feature appear labeled v′ (Fig. 1b). The only feature in the Ce 3*d* spectrum which arises solely from the Ce(IV) state and has no interference from satellite lines is the Ce $3d_{3/2}$ v‴ line (hatched) (24). For quantitative analyses, the following procedure was adopted:

(i) The total Ce 3*d* intensity was calculated by summation of the integral intensities after nonlinear subtraction of the background.

(ii) In estimating the amount of Ce(III), the reference Ce(IV) spectrum (Fig. 1a) was first scaled so that the Ce $3d_{3/2}$ v‴ (hatched) peak intensity matched that in the spectrum of the reduced catalyst (Fig. 1b).

(iii) Ce(III) in the reduced sample was calculated from the integrated intensity of the difference spectrum between those of the reduced sample (Fig. 1b) and the scaled Ce(IV) spectrum (Fig. 1a).

The validity of this procedure is supported by the difference spectrum (Fig. 1c) obtained for a reduced sample, which displayed features typical of those found for Ce(III) in passivated layers of Ce_2O_3 on Ce (25).

Temperature-programmed reaction studies were performed in a downflow reactor, designed to operate in a temperature range between −60 and 900°C and at linear temperature ramp rates of up to 30°C/min (26). A trap, containing 5 Å zeolite at dry ice temperature, removed condensable reduction products. The exit gas stream was monitored by both TCD and FID. Temperature-programmed reduction (TPR) of the precursor surface Ru carbonyl species, by 3% H_2/N_2, was measured at a ramp rate of 20°C/min on samples (50 mg), after *in situ* pretreatment in a flow of high-purity dry N_2 at ambient temperature for 0.5 h. The response of the TCD for CO and hydrocarbon was negligible at the sensitivities used, so that the TCD signal monitored H_2 uptake, and the FID signal monitored hydrocarbon formation (reported as equivalent CH_4).

Hydrogen chemisorption on supported Ru metal was performed on samples (50 mg), which were initially reduced at 350°C in the TPR apparatus and in 3% H_2/N_2 for 2 h, and then purged with dry N_2 for 1 h. The temperature of the activated sample was then allowed to fall from 350 to 200°C in N_2 before switching flow to 3% H_2/N_2. Adsorption of H_2 was monitored by TCD as the temperature fell to ambient. The system was then purged with N_2 for 30 min at ambient temperature and desorption of H_2 into flowing N_2 was monitored by TCD on ramping the temperature to 200°C at 20°C/min.

In order to examine the effect of oxidation upon Ru dispersion, further samples were reduced as above, oxidized by exposure to 1% O_2/He at 350°C for 1 h, and rereduced (r-o-r). The amount of H_2 adsorbed and then desorbed was redetermined. Reaction of the reduced precursor with O_2 was examined by H_2 titration as follows: after reduction as above, the cell temperature was adjusted to between −50 and 350°C before exposing the sample to flowing 1% O_2/He for 1 h. The extent of reaction with oxygen was then determined by TPR with 3% H_2/N_2 at a ramp rate of 20°C/min.

Fischer–Tropsch performance was assessed in a downflow microreactor, with ancillary on-line analyses capability. Prior to reaction, the catalyst precursor (∼1 g) was reduced *in situ* in pure hydrogen at 350°C for 2 h and cooled to reaction temperatures. Reaction with synthesis gas ($H_2/CO = 1.2$) at 103 kPa was studied between 240 and 300°C and at GHSV = 1500 h^{-1}.

RESULTS

Reduction of the Surface Carbonyl Complex

For the nonreducible oxides, TPR in 3% H_2/N_2 of the supported carbonyl resulted in simultaneous FID (measuring hydrocarbon evolved) and TCD (measuring H_2 reacted) profiles (Fig. 2), demonstrating that reduction of carbon-containing species was occurring. For the reducible oxides, the TCD measurement displayed two regions (Fig. 3). Region I was not accompanied by hydrocarbon formation and varied in shape from one oxide to another. Region II was accompanied by hydrocarbon formation as with the nonreducible oxides. The temperature at which the maximum rate occurred varied from 255°C for 1.8 wt% Ru/CeO_2 to 300°C for Ru/Yb_2O_3.

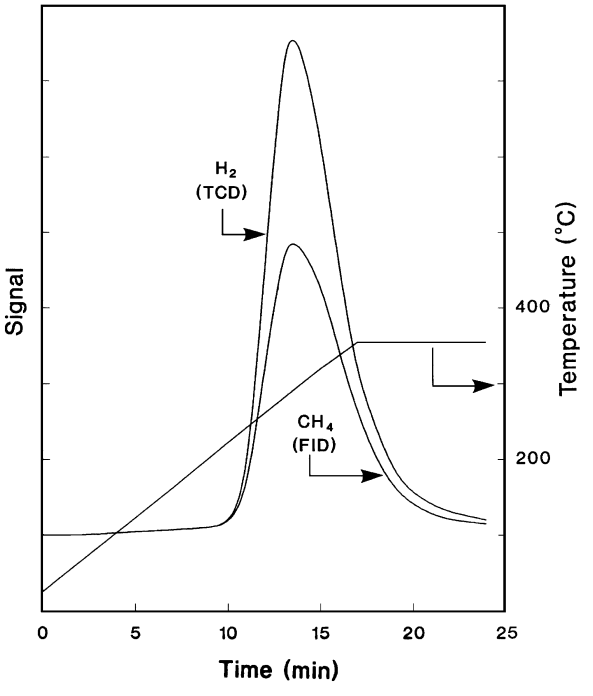

FIG. 2. TPR profile of supported 1.8% Ru/La_2O_3 precursor, showing H_2 uptake, detected by TCD, accompanied by CH_4 formation, detected by FID.

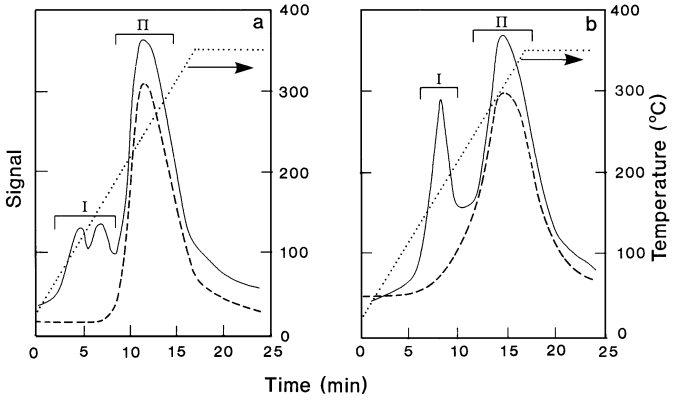

FIG. 3. TPR profiles of (a) 1.8% Ru/CeO_2 precursor and (b) 1.8% Ru/Tb_4O_7 precursor showing H_2 uptake, detected by TCD and CH_4 formation, detected by FID.

Reversible chemisorption of H_2 was observed on all the reduced Ru/rare earth oxide catalysts. After the TPR experiment, the catalyst was cooled from 250°C to ambient in 3% H_2/N_2, and the adsorption of H_2 took place, passing through a maximum rate at ca. 150°C, and had virtually ceased at 80°C (Fig. 4a). On subsequent heating in a nitrogen flow, hydrogen desorption was observed at a maximum rate at 120°C, and completed by 160°C (Fig. 4b). Table 2 lists the extent of H_2 adsorption–desorption and the corresponding Ru metal dispersions, calculated assuming that $H/Ru_{surface} = 1$. Adsorption and desorption amounts were in experimental agreement (±3%). Blank experiments with the oxide supports, in the absence of Ru, showed no uptake of H_2 under these conditions. The fraction of exposed Ru in the crystallites calculated from the H_2 adsorption–desorption data indicated a greater dispersion of Ru on cerium oxide than on the other oxides (Table 2).

La_2O_3 and CeO_2 were chosen as examples of oxide supports which were nonreducible and reducible for more extensive examination by FTIR and XPS. Reduction in H_2 (13 kPa) of the adsorbed Ru carbonyl on La_2O_3 was examined in an IR gas cell for various times at 300 and 350°C.

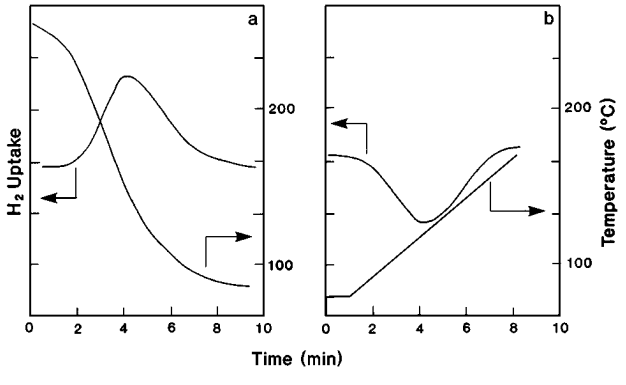

FIG. 4. (a) Adsorption and (b) desorption of H_2 on 1.8 wt% Ru/La_2O_3.

TABLE 2

Adsorption of Hydrogen on Ru Metal Supported on Rare Earth Oxides

Oxide support	Area ($m^2\ g^{-1}$)	Ru (wt%)	Pretreat	H_2 (μmol g^{-1})	Dispersion[a] (H/Ru_{total})	d (nm)
La_2O_3	54	1.8	r	19.3	0.21	6.1
			r-o-r	33.0	0.37	3.6
CeO_2	170	1.8	r	161.8	0.90	1.5
			r-o-r	162.7	0.90	1.5
Pr_6O_{11}	80	1.8	r	39.8	0.44	3.1
			r-o-r	46.1	0.51	2.7
Tb_4O_7	53	1.8	r	39.8	0.44	3.1
			r-o-r	39.8	0.44	3.1
Ho_2O_3	60	1.8	r	40.0	0.44	3.0
			r-o-r	39.8	0.44	3.0
Yb_2O_3	45	1.0	r	17.5	0.35	3.8
			r-o-r	20.7	0.41	3.2
Yb_2O_3	60	1.8	r	22.4	0.22	5.9
			r-o-r	38.3	0.43	3.1

[a] Metal dispersions were calculated assuming the ratio of hydrogen atoms to surface Ru atoms, $H/Ru_s = 1$, and Ru particle sizes from $d = 6/\rho A$ {ρ = Ru density, 12.3×10^6 g nm^{-3}, and Ru surface concentration = 1.63×10^{19} m^2 (39)}.

The initial carbonate bands arose from carbonate contamination of the support from atmospheric CO_2. These bands subsequently weakened and finally were eliminated after hydrogenation at 350°C for 1 h. Methane production during the H_2-treatment was indicated by a sharp ν(C–H) gas phase absorption band at 3020 cm^{-1} (22) and was accompanied by the disappearance of the carbonyl and carbonate bands. GC analysis of the gas phase after hydrogenation at 120 and 300°C (Table 3) confirmed the generation of CH_4 at 300°C, while at 120°C, traces of C_2H_6 and C_3H_8 were also detected. For 1.8 wt% Ru/La_2O_3, quantitative estimation of the amount of CH_4 produced at 300°C in the gas cell gave CH_4/Ru of about 4.

Reduction of the dicarbonyl on La_2O_3 and CeO_2 (1.8 wt% Ru), in 3% H_2/N_2 at 350°C for 20 min in an *in situ* reaction cell, resulted in a shift of the Ru $3d_{5/2}$ binding energy from 282.0 and 281.8 eV to 280.1 and 280.2 eV, respectively (Figs. 5 and 6). Approximately 35% reduction to

TABLE 3

Analysis of Reduction Products of Ru Carbonyl Supported on La_2O_3[a]

Temperature (°C)	Ru in disc	C reduced	Gas phase analysis (wt%)		
			CH_4	C_2H_6	C_3H_8
120	39.5[b]	15[b]	95	3	2
300	32.5	130	100	—	—

[a] Gas chromatographic analysis after heating sample in 13.1 kPa H_2 for 1 h, 1.8 wt% Ru metal loading.

[b] Ru containing (mmol).

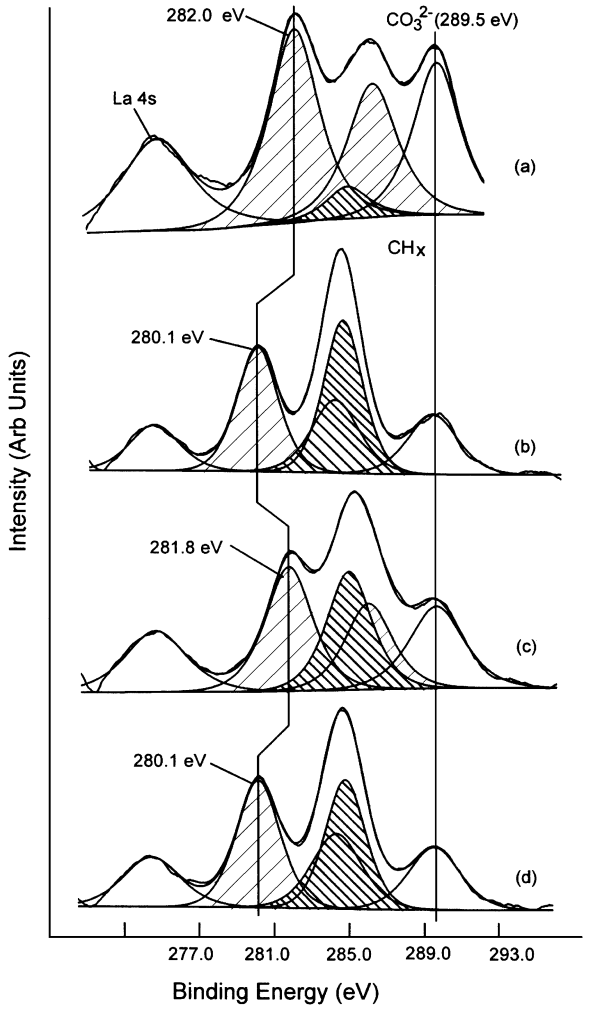

FIG. 5. XPS spectra of 1.8 wt% Ru/La_2O_3: (a) precursor *in vacuo*; (b) after reduction in 3% H_2 at 350°C for 20 min; (c) product from (b) was oxidized in 1% O_2/He at 150°C for 20 min; (d) product from (c) was reduced in 3% H_2 at 350°C for 20 min (the Ru $3d_{5/2}$–$3d_{3/2}$ envelope is hatched).

Ce(III), giving an overall bulk oxide composition of $CeO_{1.83}$, was observed for ceria. This stoichiometry corresponded well with the O/Ce ratio of ~1.76, calculated from the O 1*s* region (Table 4), and further supports the procedures adopted for analysis of the Ce spectra. In contrast, reduction of the high area ceria itself at 350 and 500°C in 3% H_2/N_2 for 20 min yielded only 17% ($CeO_{1.92}$) and 27% ($CeO_{1.87}$) Ce(III), respectively (9).

Oxidation of Supported Ru Catalysts

The reduced catalysts were highly susceptible to oxidation by 1% O_2/He, even at subambient temperatures. During TPR of 1.8 wt% Ru/La_2O_3 in 3% H_2/N_2, which had been oxidized in flowing 1% O_2/He at −50, 23, 200, 300, or 350°C, more than one type of oxidized species was apparent. The TPR profiles of oxidized catalysts consisted of a single reduction peak centered on 80°C (Figs. 7a–7c), together with a shoulder near 110°C, which increased in intensity as the temperature of initial oxidation treatment increased. The total H_2 uptake gave a O/Ru stoichiometry of 2.0 (Table 5), showing oxidation of Ru metal to RuO_2 except at −50°C. Similar results were obtained for supported Ru on Ho_2O_3 and Yb_2O_3.

With La_2O_3, at 4.5 wt% Ru loading, and for longer reaction times, the TPR shoulder at 110°C developed into a separate, distinct peak (Figs. 7d and 7e). The two peaks showed changes in the relative intensities after oxidation over different periods of time. When the oxidation time was extended to 6 h, the peak at 80°C decreased, while that at 110°C first increased but then also decreased (Fig. 7d and Table 5), such that the total H_2 uptake fell from the initial 9.0 through 8.2 to 6.2×10^{-4} mol g^{-1} of catalyst. After

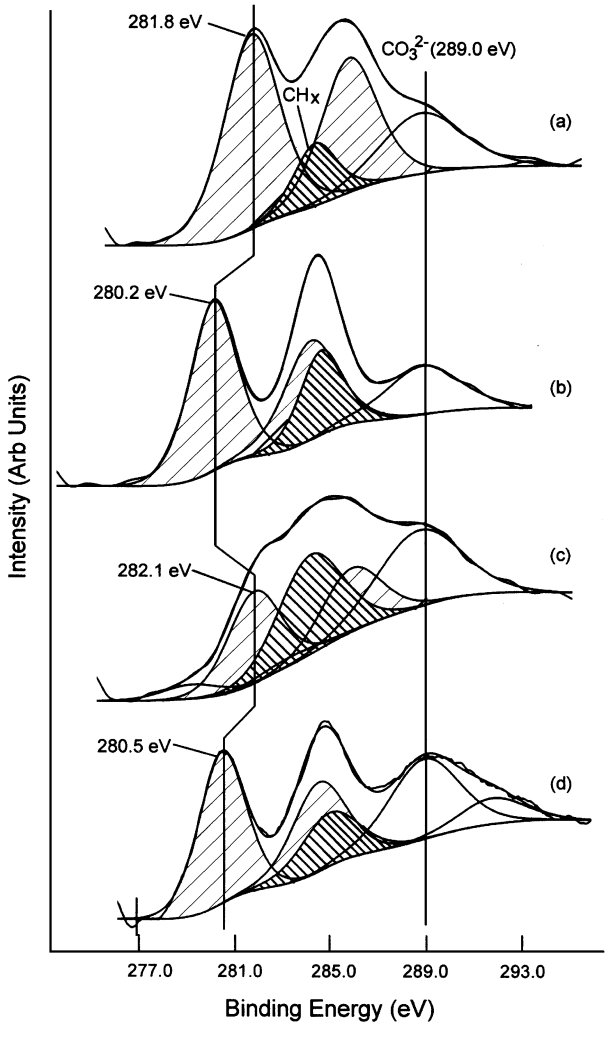

FIG. 6. XPS spectra of 1.8 wt% Ru/CeO_2; (a) precursor *in vacuo*; (b) after reduction in 3% H_2 at 350°C for 20 min; (c) product from (b) was oxidized in 1% O_2/He at 150°C for 20 min; (d) product from (c) was reduced in 3% H_2 at 350°C for 20 min. Hatched peaks are attributed to Ru $3d_{5/2}$ signals.

TABLE 4

XPS Atomic Ratios for 1.8 wt% Ru/Rare Earth Oxide[a]

Support	Treatment	Ru/RE[b]	Carbonate/RE[a]	O^{2-}/RE[c]	OH^-/RE[d]
La_2O_3	Reduced[e]	0.07	0.29	0.36	1.12
	Oxidised[f]	0.06	0.34	0.63	0.21
	Reduced[e]	0.07	0.30	0.49	0.88
CeO_2	Reduced[e]	0.15	0.31	1.76	0.21
	Oxidised[f]	0.13	0.39	2.63	0.32
	Reduced[e]	0.08	0.21	1.62	0.48

[a] Intensities, except for La and Ce, calculated from curve fitting the O 1*s* and Ru 3*d*/C 1*s* regions; atomic ratios (±15%) calculated with respect to La 3*d* or Ce3*d*.

[b] From Ru 3*d* peak area.

[c] From O 1*s* at 528.3 eV ($La_2\underline{O}_3$), 529.5 eV (La$\underline{O}$OH) or 529.5 eV ($Ce\underline{O}_2$).

[d] From O 1*s* at 531.2 to 532.0 eV ($\underline{O}H$ and CO_3^{2-}) for CeO_2 and peak at 531.5 ($La(OH)_3$) or La_2O_2.

[e] In 3% H_2/N_2 at 350°C for 20 min.

[f] In 1% O_2/He at 150°C for 20 min.

treatment at 350°C for 6 h, a brown–yellow film, ascribed to free RuO_2, was found deposited in the cooler region downstream of the reactor (28, 29).

In XPS experiments, reoxidation of the reduced 1.8 wt% Ru/La_2O_3 in 1% O_2/He at 150°C for 20 min led to a shift of the Ru $3d_{5/2}$ peak from the Ru metal value at 280.1 eV to that typical of hydrated RuO_2 at 281.8 eV (17), confirming ready oxidation of supported Ru metal (Fig. 6c). As expected subsequent reduction reversed this shift. Furthermore, no change was detected in the Ru/La ratio, indicating that there was neither loss of Ru nor change in dispersion under mild oxidation conditions (Table 4). In the r-o-r cycle, there was a substantial increase in hydroxyl concentration after each reduction step with a concomitant decrease in the O 1*s* peak assigned to carbonate oxygen. After the initial reduction, the carbonate/La ratio remained constant during r-o-r cycling.

By contrast, hydrogen uptake for the reducible oxides was much greater. TPR profiles, obtained for oxidized 1.8 and 5 wt% Ru/CeO_2, are shown in Figs. 8f and 8g. With Ru/CeO_2, the TPR experiment was started at 0°C, as hydrogen uptake began immediately upon exposure of oxidized specimens at ambient temperature. The total hydrogen uptake, on heating between 0 and 300°C, considerably exceeded that required for reduction solely of supported RuO_2 to Ru metal; the amount of hydrogen uptake was sufficient to reduce bulk cerium oxide from an initial stoichiometry of CeO_2 to $CeO_{1.86}$ (Table 6).

TPR profiles of oxidized 1.8 wt% Ru supported on praseodymium and terbium oxide are shown in Figs. 8b and 8d, together with profiles for the parent oxides in the absence of Ru (Figs. 8a and 8c). The small shoulder (marked ∗ in Fig. 8b) on the peak in the TPR on praseodymium oxide fulfils the total requirement for stoichiometric reduction of Ru(IV) and the main peak observed (at 140°C)

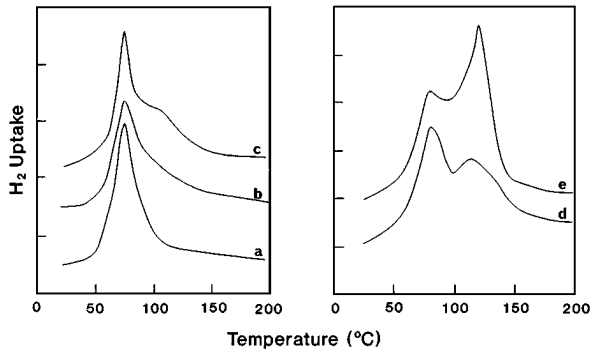

FIG. 7. Effect of oxidation in 1% O_2/He on TPR profiles of 1.4 wt% Ru/La_2O_3 for 1 h at (a) 200°C, (b) 300°C, and (c) 350°C, and for 4.5 wt% Ru/La_2O_3 at 350°C for (d) 6 h and (e) 2 h.

represents quantitative reduction of $PrO_{1.83}$ (i.e., Pr_6O_{11}) to $PrO_{1.45}$ (i.e., approximately Pr_2O_3), within experimental error. In contrast, TPR examination of praseodymium oxide alone (Fig. 8a) showed two features at much higher temperature, namely, a well-defined peak at 480°C, with a shoulder at 420°C. After total reduction, the stoichiometry approached $PrO_{1.5}$, with possible intermediate formation of $PrO_{1.71}$ (28) leading to the observed shoulder at 420°C. Similarly, terbium oxide alone showed a TPR peak at 480°C and shoulder at 410°C (Fig. 8c) and the single peak at 110°C observed for Ru/terbium oxide was found to exceed that for reduction of Ru(IV) to Ru(0), as shown in Table 6.

After oxidation (1% O_2/He, 20 min, 150°C) of reduced 1.8 wt% Ru/cerium oxide, an increase in the Ru 3*d* binding energy from 280.2 to 282.1 eV, attributed to oxidation of Ru metal and no Ce(III), was detected, indicating that the cerium oxide had been oxidized to CeO_2 (31). Subsequent reduction of the oxidized material resulted in no significant

TABLE 5

Temperature Programmed Reduction of Oxidised Ru Metal Supported on La_2O_3[a]

Ru (wt%)	Oxidation (°C)	H_2 uptake(mmole g^{-1}) peak position 80°C	110°C	O/Ru ratio
1.8	−50	324	—	1.8
1.8	23	384	—	2.1
1.4	200	279	—	2.0
1.4	300	272	sh	2.0
1.4	350	280	sh	2.0
4.5	350[b]	400	500	2.0
4.5	350[c]	280	540	—
4.5	350[d]	240	380	—

[a] Pretreatment: Reduce precursor in 3% H_2/N_2 for 2 h at 350°C, oxidize 1% O_2/He for 1 h at indicated temperature, flush with N_2.

[b] 2 h oxidation.

[c] 4 h oxidation.

[d] 6 h oxidation.

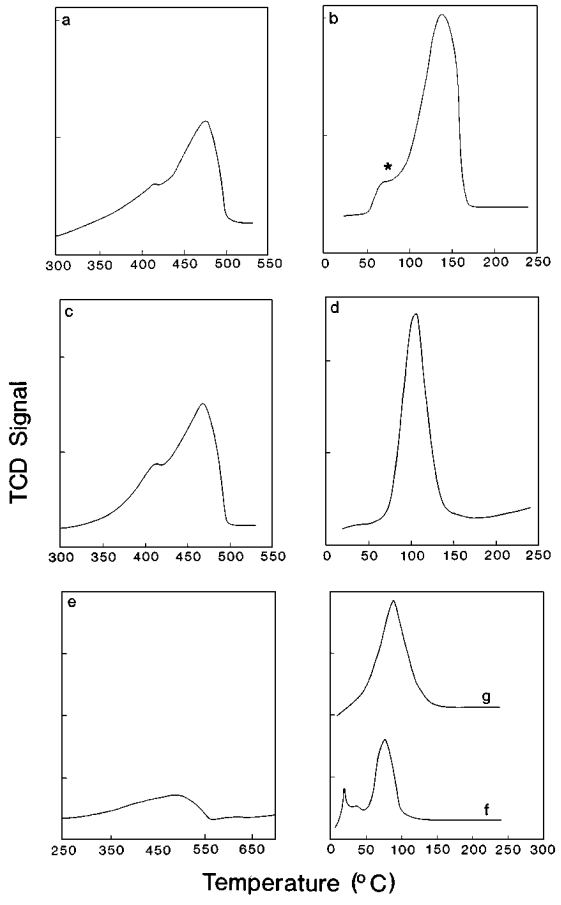

FIG. 8. TPR profiles of (a) Pr_6O_{11}, (b) oxidized 1.8 wt% Ru/Pr_6O_{11}, (c) Tb_4O_7, (d) oxidized 1.8 wt% Ru/Tb_4O_7, (e) CeO_2, (f) oxidized 1.8 wt% Ru/CeO_2, and (g) oxidized 4.5 wt% Ru/CeO_2.

changes to the Ru/Ce ratio (Table 4), and the Ru binding energy and the stoichiometry, $CeO_{1.82}$, were the same as those following the reduction of the precursor (Table 4 and Fig. 8d).

Fischer–Tropsch Performance

At the initial stage of reaction, the product stream consisted mainly of CH_4 and CO_2. Higher hydrocarbons then gradually appeared over supported Ru on La_2O_3, Ho_2O_3, CeO_2, Pr_6O_{11}, and Tb_4O_7 after 30 min. However, only CH_4 was observed over Ru/Yb_2O_3. This selectivity (Table 7) persisted virtually unchanged over the period of study. The activity of the catalyst after 30 min, as given in Table 8, decreased by about 30% over the next 5 h, before leveling off, and stabilized for at least 15 h.

DISCUSSION

Reduction of Supported Ru Carbonyls

In TPR experiments surface Ru carbonyls on all the rare earth oxides were readily reduced by 3% H_2/N_2 at 250–300°C with formation of CH_4 (Figs. 2 and 3; Table 3). Similar reduction of ligands with formation of CH_4 has been reported previously for a number of carbonyl complexes on γ-Al_2O_3 (32). In the absence of surface ruthenium, reduction of surface carbonate species was not observed up to the decomposition temperature of the carbonate (31). This result parallels a report by Bernal *et al.*, who showed that supported metallic Rh/La_2O_3 catalyzed reduction of surface carbonate (34). Such processes presumably involve spillover of hydrogen atoms from small metal particles to the support. Reduction of supported-Ru/reducible oxide precursors in 3% H_2/N_2 occurred over two distinct temperature regions, the first involving only uptake of H_2 (Fig. 3, Region I), and the second involving H_2 uptake accompanied by liberation of CH_4 (Region II). Hydrogen uptake was not observed below 250°C in the TPR of the reducible oxide supports in the absence of ruthenium and was not present in TPR of precursors on the nonreducible oxides. For the reducible oxides, the H_2 uptake for region I exceeded that

TABLE 6

Temperature-Programmed Reduction of Oxidized Catalysts[a]

Oxide	Ru (wt%)	H_2 (mmol g^{-1})	MO_{y-x}[b] $(y-x)$
CeO_2	0.0	0.53[c]	1.91
	1.8	1.18	1.86
	5.0	1.78	1.87
Pr_6O_{11}	0.0	1.88[c]	1.51
	1.8	2.58	1.45
Tb_4O_7	0.0	2.39[c]	1.30
	1.8	1.83	1.48

[a] Pretreatment: Precursor Ru carbonyl species reduced at 350°C in 3% H_2/N_2 for 1 h, then oxidized in 1% O_2/He for 1 h, flushed with N_2, and cooled before running TPR in 3% H_2/N_2.

[b] Stoichiometry of reduced support assuming total H_2 is given by

$$RuO_2 + 2H_2 \rightarrow Ru + 2H_2O$$
$$\text{and} \quad MO_y + xH_2 \rightarrow MO_{y-x} + xH_2O$$

[c] Reduction of support as measured by TPR to 550°C.

TABLE 7

Selectivity of Ru Supported on Rare Earth Oxides

Support	Ru (wt%)	Conv. %	C_1	C_{2-5}	C_{6+}	$\%C_{2-5\ ene}$
La_2O_3	1.8	24	42	48	10	15.5
	4.5	43	38	54	9	6.5
Ho_2O_3	1.8	23	65	31	4	8.3
	4.5	33	56	38	6	5.2
Yb_2O_3	1.0	52	100	0	0	0
CeO_2	1.8	6	17	61	22	55.3
	5.0	15	23	59	18	51.1
Pr_6O_{11}	1.8	7	25	61	13	46.9
Tb_4O_7	1.8	13	40	50	10	16.5

TABLE 8

Activity of Supported Ru/Rare Earth Oxides

Support	Ru (wt%)	Rate[a] to CO_2	TOF (10^{-3} s^{-1})	Rate[a] to HC	TOF (10^{-3} s^{-1})
La_2O_3	1.8	0.25	6.7	0.91	24.3
	4.5	0.87	13.0	1.65	24.7
Ho_2O_3	1.8	0.12	1.5	0.86	11.0
	4.5	0.42	2.4	1.24	7.1
Yb_2O_3	1.0	—	—	1.94	5.4
CeO_2	1.8	0.33	2.1	0.25	1.6
	5.0	0.70	1.7	1.16	2.8
Pr_6O_{11}	1.8	0.21	2.7	0.25	3.2
Tb_4O_7	1.8	0.23	3.0	0.49	6.1

[a] μCO: g^{-1} cat s^{-1}.

required for the reduction of a Ru species, suggesting reduction of the support by spillover of hydrogen from surface Ru(O∼). Although the bulk Ru is present as $Ru(CO)_n$ below 200°C, because the catalyst precursor has been evacuated, the presence of some Ru(O∼) species formed by progressive vacuum removal of CO ligands is possible. Calculations, based on support reduction in Region I, afford stoichiometries of $CeO_{1.79}$, $PrO_{1.54}$, and $TbO_{1.53}$, assuming initial stoichiometries of CeO_2, $PrO_{1.83}$ (i.e., Pr_6O_{11}), and $TbO_{1.75}$ (i.e., Tb_4O_7). It is of interest to note that the value for reduced cerium oxide is nearly the same as that calculated from XPS results, after H_2 reduction of the Ru-containing precursor (Table 6). Our results on the TPR of $PrO_{1.83}$ agree well with those of Fierro and Olivan (35).

A previous TPR study on CeO_2 support itself has revealed that uptake of H_2 is complex and contains a surface area dependent component (9). A temperature of 550°C was required to achieve a surface stoichiometry of $CeO_{1.82}$ on samples of cerium oxide with the same surface area as that used here in reactions with $Ru_3(CO)_{12}$; the average bulk stoichiometry under those conditions was $CeO_{1.91}$ (Table 6); final reduction toward $CeO_{1.5}$ was still in progress at 800°C (9). Our XPS results for the support itself yield stoichiometries of $CeO_{1.92}$ for reduction at 350°C and $CeO_{1.87}$ at 500°C and are similar to the TPR data. The XPS data closely represent bulk analyses, since the particle size of cerium oxide with surface area of 170 m^2 g^{-1} is ∼5 nm (9) from TEM observations. These results further show that reduction of cerium oxide at 350°C resulted in more extensive reduction of the support (to $CeO_{1.82}$) in the presence of Ru than in its absence. Considering differences in experimental conditions, the correspondence of the values calculated from TPR and XPS is noteworthy.

The greater degree of reduction of reducible oxides in the presence of Ru can be ascribed to dissociative chemisorption of H_2 on Ru species, leading to spillover reduction of the support oxide. Whether, in the case of the initial precursor reduction corresponding to Region I in Fig. 3, such a process can occur with the surface Ru carbonyl species itself or whether a trace amount of precursor has already decomposed with formation of clusters of Ru metal has not been established although Ru metal was not noted by XPS prior to reduction. An earlier XPS study of $Ru_3(CO)_{12}$ on low area cerium oxide (1 m^2 g^{-1}) reported Ce(IV) reduction corresponding to a final stoichiometry of $CeO_{1.79}$ following exposure to synthesis gas ($H_2/CO = 1$) at 350°C (36). Similarly, in a TPR study of Ni supported on CeO_2, coreduction of the support has been reported, resulting in an oxide stoichiometry of $CeO_{1.85}$ at 400°C (37). In TPR studies of Pd on CeO_2, $PrO_{1.83}$, and $TbO_{1.75}$, each preparation showed uptake of H_2 in excess of that for reduction of Pd species and which was therefore attributed to reduction of the support, but the level of reduction was not determined (38).

Chemisorption of hydrogen was found to occur at about 100°C from 3% H_2/N_2. The data for H_2 adsorption in Table 2 show high dispersion for Ru metal on each of the supports, with the greatest value, 0.90, found on the highest area support, namely cerium oxide (170 m^2 g^{-1}). The values on Tb and Pr are lower (0.4) and comparable to those found for Ru supported on M_2O_3 (M = La, Ho, Yb). Koopman *et al.* have demonstrated that, with Ru/SiO_2, a similar dynamic procedure to that adopted here gives satisfactory agreement with measurements by static chemisorption at 63°C (39).

Oxidation of Reduced Catalyst

The reduced catalysts were very susceptible to quantitative oxidation to RuO_2. The results in Table 5 demonstrate that even at −50°C, almost complete conversion to RuO_2 is effected on La_2O_3 in 1% O_2/He. At 23°C and higher temperatures, oxidation of supported Ru metal to supported RuO_2 was indeed complete. Hydrogen reduction of the supported RuO_2 (Fig. 8) was particularly facile, occurring at a substantially lower temperature than the 170°C reported for unsupported RuO_2 (36, 40). Similarly, reduction profiles as low as 87°C have been reported by Bossi *et al.* for Ru/MgO after reduction–oxidation–reduction cycles (41).

Depending upon oxidation conditions, two different reduction maxima were observed, at 80 and 110°C, with the higher temperature reduction peak increasing in magnitude with the severity of oxidation (Table 5 and Fig. 7). Two-stage reduction of surface RuO_2, for example, via Ru(+III) or Ru(+II) species, should give constant peak ratios and so cannot explain adequately the variation in intensities of the 80 and 110°C reduction profiles. A bimodal variation in RuO_2 crystallite size, with one state approaching bulk RuO_2 in nature, would give rise to two maxima of variable magnitude, as has been observed with silica-supported Ir and Pt/Ir catalysts (41). Only under the most severe oxidation conditions (350°C for 6 h) was there actual physical loss of RuO_2 from the catalyst bed.

With Ce, Pr, and Tb, the reduced Ru/rare earth oxide systems underwent facile oxidation. However, in contrast to the nonreducible oxides, the resultant TPR profiles of the oxidized catalysts (350°C, 1% O_2/He) revealed a very large uptake of H_2 (Table 6), attributable to rereduction of the support in addition to the reduction of Ru(IV) to Ru(0). Thus, in the case of cerium and praseodymium, this mild oxidation restored virtually the full oxygen stoichiometry of the rare earth oxide to that prior to initial reduction, i.e., corresponding to that of treatment in air at 600°C. Indeed, XPS results indicate that oxidation of Ce(III) to Ce(IV) was complete at 150°C within 20 min.

The binding energies of the precursors and oxidized Ru/rare earth oxides were higher than those reported for Ru(IV) in anhydrous RuO_2 (280.9) and hydrated RuO_2 (281.5) but lower than that reported for Ru(VI) in RuO_3 surface phases on either hydrated or anhydrous RuO_2, which fall in the range 282.6 to 283.2 (17). For this reason they have been assigned to Ru(IV), where local surface interaction with carbonate and hydroxyl groups has elevated the binding energy. Further evidence to support the assignment of Ru(IV) comes from the TPR of the oxidized catalysts (Table 6). In the case of oxidized Ru/La_2O_3 the H_2 uptake indicated a Ru : O ratio of 0.5. For Ru/CeO_2, if the H_2 uptakes of the 1.8 and 5 wt% loadings are compared, and assuming the same degree of reduction of the ceria support, then the difference in going from 1.8 to 5 wt% loading (0.031 mol/g Ru) requires 0.06 mol H_2, giving a Ru : O ratio of 0.5. Thus the Ru species on the oxidized catalyst must be Ru(IV), but shifted to higher binding energies due to ligand effects. Finally, it could be questioned how surface hydroxyl groups would be present on the ceria and lanthana given that the oxidation is in a 1% O_2/He stream. Ceria is well known to form a bronze phase with hydrogen (44), as was evident with a significant hydroxyl (also carbonate) component after reduction (Table 4). These surface hydroxyl groups still persist through the oxidation stage and are responsible for the modification in binding energy. A similar situation exists for the lanthana, but in this case, the level of surface carbonate is larger. High binding energies for supported Ru attributed to the effects of ligands have also been observed by other workers; Aika *et al*., for example, measured $3d_{5/2}$ binding energies between 282.0 and 283.0 eV for Ru(III) on alkaline earth supports and attributed such values to coordination changes of the surface species (18). Bossi *et al*. observed higher binding energies for Ru/Al_2O_3 than other workers and attributed the shift to interaction with the support (42). In the case of Ru/cerium oxide, the high value may be due to the presence of ligands on the Ru, such as OH^- or CO_3^{2-}, which have been reported to increase the Ru binding energy over that of the oxide (17, 43). Substantial metal–support surface interaction is not surprising considering the high Ru dispersion observed on CeO_2.

Reduction of Oxidized Catalyst

For the sesquioxides, where no reduction of the support was involved, reduction of Ru(IV) on the oxidized samples to Ru metal occurred at temperatures lower than 110°C. The process of (r-o-r) did not greatly alter the Ru dispersion on the oxides of Ce, Pr or Tb, in contrast to the increase in dispersion found for La and Yb (Table 2).

It is noteworthy that r-o-r results in a large decrease in the Ru/Ce ratio as observed by XPS (Table 4), whereas there is a much smaller corresponding decrease in H_2 adsorption capacity. The XPS result would normally be interpreted as implying a large increase in metal particle size leading to attenuation of signal. However, at the particle sizes of 1.5–3 nm implied by the H_2 adsorption results (Table 2), little of the XPS signal intensity should be attenuated by the Ru particles themselves. As the decrease in XPS signal results neither from a loss of Ru from the system nor from a decrease in metal dispersion, it appears therefore that the XPS change requires a relative increase in Ce signal. This is believed to arise through decoration or burial of Ru by Ce species, without limiting accessibility of H_2 to the Ru particles, due to the solubility of hydrogen in the reduced cerium oxide lattice (9, 35). In contrast, no substantial attenuation of the Ru XPS signal occurred after r-o-r in the case of supported Ru/La_2O_3, implying the absence of decoration of Ru by the support.

Among the rare earth oxides used as supports, reducible oxides exhibit higher selectivity for alkene, indicating low hydrogenation activity. Lower alkene production in excess of 50 wt% of hydrocarbon product was obtained using CeO_2 as a support.

CONCLUSION

Heating in H_2 leads to simultaneous reduction of ruthenium carbonyl species and a spillover reduction of surface carbonate, with evolution of CH_4 and formation of clusters of Ru metal on the support. Reversible chemisorption of hydrogen on the reduced Ru catalysts was observed with a maximum rate at about 120°C. The data for H_2 adsorption show metal dispersions of up to 90%. The reduced catalysts are very susceptible to oxidation and severe oxidation conditions can cause physical loss of RuO_2 from the catalyst. Spillover reduction of catalyst support was observed for reducible oxides but not the nonreducible oxides. CeO_2 and Pr_6O_{11} proved effective supports for lower olefin production.

REFERENCES

1. Vannice, M. A., and Garten, R. L., *J. Catal.* **63**, 255 (1980).
2. Kugler, E. L., *Amer. Chem. Soc. Symp. Div. Petrol. Chem.,* 564 (1980).
3. Morris, S. R., Moyes, R. B., Wells, P. B., and Whyman, R., *Stud. Surf. Sci. Catal.* **11**, 247 (1982).

4. Goodwin, J. G., Jr., Chen, Y. W., and Chuang, S. C., *in* "Proc. Symp. Catal. Convers. Synth. Gas Alcohols Chem." (R. G. Herman, Ed.), p. 179. Plenum, New York, 1983.
5. Uchiyama, S., and Gates, B. C., *J. Catal.* **110**, 388 (1988).
6. Pierantozzi, R., *Chem. Ind.* **22**, 115 (1985).
7. Kikuchi, E., Nomura, H., Matsumoto, M., and Morita, Y., *Appl. Catal.* **7**, 1 (1983).
8. Bruce, L. A., Hughes, A. E., Hoang, M., and Turney, T. W., *Appl. Catal. A* **100**, 51 (1993).
9. Bruce, L. A., Hughes, A. E., Hoang, M., and Turney, T. W., *Appl. Catal. A* **134**, 351 (1996).
10. Bruce, L. A., Hughes, A. E., Hoang, M., and Turney, T. W., *Inorg. Chim. Acta* **254**, 37 (1997).
11. Bruce, L. A., Hardin, S., Hoang, M., and Turney, T. W., *J. Mater. Chem.,* 423 (1991).
12. Bruce, L. A., Hardin, S., Hoang, M., and Turney, T. W., *Aust. J. Chem.* **4**, 645 (1991).
13. Eady, C. R., Jackson, P. F., Johnson, B. F. G., Lewis, J., Malatesta, M. C., McPartlin M., and Nelson, W. J. H., *J. Chem. Soc. Dalton Trans.*, 383 (1980).
14. Gonzalez-Elipe, A. R., Espinos, J. P., Fernandez, A., and Munuera, G., *Appl. Surf. Sci.* **45**, 103 (1990).
15. Hughes, A. E., and Sexton, B. A., *J. Electron Spectrosc. Relat. Phenom.* **46**, 31 (1988).
16. Siegbahn, K., *Philos. Trans. Roy. Soc. London A* **268**, 33 (1979).
17. Demanet, C. M., *S.-Afr. Tydskr. Chem.* **35**(2), 45 (1982).
18. Malitesta, C., Morea, G., Sabbatini, L., and Zambonin, P. G., *Chimica* **78**, 473 (1988).
19. Aika, K., Ohya, A., Ozaki, A., Inoue, V., and Yosumori, I., *J. Catal.* **92**, 305 (1985).
20. Mårtensson, N., and Nyholm, R., *Phys. Rev. B* **24**(12), 7121 (1981).
21. Jørgensen, C. K., and Berthou, H., *Chem. Phys. Lett.* **13**(3), 186 (1972).
22. Uwamino, Y., Ishizuka, T., and Yamatera, H., *J. Electron Spectrosc. Relat. Phenom.* **34**, 67 (1984).
23. Perry, D. L., Tsao, L., and Brittain, H. G., *J. Mater. Sci. Lett.* **3**, 1017 (1984).
24. Imada, S., and Jo, T., *Physica Scripta* **41**, 115 (1990).
25. Le Normand, F., Hilaire, L., Kili, K., Krill, G., and Maire, G., *J. Phys. Chem.* **92**, 2561 (1988).
26. Barr, T. L., *in* "Electron Spectroscopy for Chemical Analysis Examination of Rare Earth and Near Rare Earth Species. Quantitative Analysis of Materials, ASTM STP643" (N. S. McIntyre, Ed.), p. 83; *ASTM Spec. Tech. Publ.* 1978.
27. Bruce, L. A., Mole, T., and Turney, T. W., Natl. Energy Res. Develop. Demonst. Prog., Report No. EG86/566, Dept. Prim. Indust. & Energy, Canberra, 126 (1986).
28. Kwok, J., and Robinson, G. W., *J. Chem. Phys.* **36**, 3139 (1962).
29. Shelef, M., and Gandhi, H. S., *Platinum Met. Rev.* **18**, 1 (1974).
30. Gandhi, H. S., Stepien, H. K., and Shelef, M., *Mater. Res. Bull.* **10**, 837 (1975).
31. Kordis, J., and Eyring, L., *J. Phys. Chem.* **72**, 2044 (1968).
32. Tsisun, E. L., Nefedov, B. K., Shapiro, E. S., Antoshin, G. V., and Minachev, K. M., *React. Kinet. Catal. Lett.* **24**, 37 (1984).
33. Hucul, D. A., and Brenner, A., *J. Amer. Chem. Soc.* **103**, 217 (1981).
34. Foger, K., Hoang, M., and Turney, T. W., *J. Mater. Sci.* **27**, 77 (1992).
35. Bernal, S., Botana, F. J., Ramirez, F., and Rodriguez, J. M., *Appl. Catal.* **31**, 267 (1987).
36. Fierro, J. L. G., and Olivan, A. M., *J. Less Common Metals* **107**, 331 (1985).
37. McNicol, B. D., and Short, R. T., *J. Elect. Chem.* **92**, 115 (1978).
38. Barrault, J., Alouche, A., Paul-Boncour, V., Hilaire, L., and Percheron-Guegan, A., *Appl. Catal.* **46**, 269 (1989).
39. Le Normand, F., Barrault, J., Breault, R., Hilaire, L., and Kiennemann, A., *J. Phys. Chem.* **95**, 257 (1991).
40. Koopman, P. G. J., Kieboom, A. P. G., and Bekkum, H., *J. Catal.* **69**, 172 (1981).
41. Bossi, A., Cattalani, A., Garbassi, F., Petrini, G., and Zanderighi, L., *J. Thermal Anal.* **26**, 8 (1983).
42. Foger, K., and Jaeger, H., *J. Catal.* **70**, 63 (1981).
43. Bossi, A., Garbussi, F., Orlandi, A., Petrini, G., and Zanderighi, L., *Stud. Surf. Sci. Catal.* **3**, 405 (1979).
44. Kim, K. S., and Winograd, N., *J. Catal.* **35**, 66 (1974).
45. Fierro, J. L. G., Soria, J., and Rojo, J. M., *J. Solid State Chem.* **66**, 154 (1987).